Engineering and Technology Journal
Journal homepage: https://etj.uotechnology.edu.iq

Assessment of flash flood detection in Erbil city using change detection indices for SAR images

Abbas Mohammed Noori[a,b*], **Abdul Razzak T. Ziboon**[c], **Amjed N. AL-Hameedawi**[a]

[a] Civil Engineering Dept., University of Technology-Iraq, Alsina'a street, 10066 Baghdad, Iraq.
[b] Department of Surveying Engineering, Technical Engineering College of Kirkuk, Northern Technical University, Kirkuk 36001, Iraq.
[c] College of Engineering, Al-Esraa University, Baghdad, Iraq.
[*]Corresponding author E-mail: bce.23.43@grad.uotechnology.edu.iq , abbasnoori@ntu.edu.iq

HIGHLIGHTS

- Flash flood maps were created using NCI and RI algorithms across the region
- Open-source SAR data and Snap 9.0 software addressed cloud cover and vegetation issues in flood mapping
- The accuracy of NCI and RI algorithms for flash flood detection was evaluated
- Simple, efficient algorithms provided good accuracy for flood monitoring in large areas, like the entire city of Erbil

ARTICLE INFO

Handling editor: Mahmoud S. Al-Khafaji

Keywords:

Floods; Normalized change indiex; Ratio index; Infrastructure; SAR image.

ABSTRACT

The frequency and intensity of flash floods are expected to increase due to climate change, resulting in significant casualties and damage to infrastructure and the economy. Reliable and timely flood maps are essential for an effective disaster management plan. On December 17, 2021, a severe flash flood in Erbil City resulted in twelve fatalities and extensive damage to the affected area. The ability of synthetic aperture radar (SAR) images to penetrate clouds and heavy precipitation is vital for accurate flood imaging. This study analyzed Sentinel-1 satellite-based radar images before and after the flood to detect the inundation. Two change detection techniques, the Normalized Change Index (NCI) and the Ratio Index (RI), combined with semi-automatic thresholding were employed. Both methods successfully identified the flooded region with consistent findings. The overall accuracy of NCI and RI were 90.5% and 84.3% respectively. The accuracy assessment revealed that the NCI method outperforms the RI method in detecting the flash flood event in Erbil City. This model is viable for disaster management, enabling the evaluation of damage to critical municipal infrastructure and other assets, thus supporting effective urban governance and timely response to emergencies. At the final stage of disaster management, this model can be implemented to evaluate the extent of loss on major municipal infrastructure and other properties within the area.

1. Introduction

Worldwide flood disasters are becoming more likely due to climate change and growing urbanization [1]. Global climate change greatly affects the resilience and vulnerability of Earth's ecosystem [2]. However, the most important meteorological components are precipitation and temperature, which profoundly impact ecosystems [3]. A key objective outlined in the Sustainable Development Goals (SDGs) established by the United Nations is to understand the causes and consequences of droughts and floods and their correlation with climate change [4]. Additionally, it is imperative to identify and evaluate the risks associated with these natural hazards at various levels. Floods are recognized as significant challenges that can hinder the attainment of SDGs, particularly in ensuring universal access to sustainable water management and sanitation. Floods can contaminate water sources and cause damage to infrastructure. Therefore, it is crucial to manage floods effectively to achieve the SDGs successfully.

Few natural disasters are as widespread or destructive as floods, which devastate lives and economies worldwide [5,6]. The effects of flooding in vulnerable places will worsen due to population growth, urbanization, and changes in precipitation patterns [7,8]. Flooding can be caused by prolonged, extreme precipitation, thawing snow, dam collapse, and frozen lake overflow [9,10]. Most flooding happens in rural regions, but the recent trend toward urbanization increases the likelihood that floods in urban areas will be catastrophic [6]. Flash floods occur suddenly and often last less than six hours. Weather predictions are now the only form of warning, but they are unreliable and too general to be useful in preparing for flooding events.

A combination of factors, including growing urban populations and altered weather patterns, may explain why flash floods have become more common in recent years in Erbil City. Particularly in 2021 and 2022, the floods in Erbil City severely

http://doi.org/10.30684/etj.2024.151205.1777
Received 25 June 2024; Received in revised form 07 August 2024; Accepted 10 August 2024; Available online 23 September 2024
2412-0758/University of Technology-Iraq, Baghdad, Iraq

devastated homes, cars, and people. Overnight on 17 December 2021, Erbil received between 59 and 60 millimeters of rain, according to the Regional Directorate General of Meteorology and Seismology [11]. Twelve people lost their lives, and the damage was fifteen million dollars [12]. More than 2,509 homes and 867 vehicles were impacted by the flood [12]. Hence, monitoring floods plays a crucial role in mitigating the risk associated with flooding. Detecting the state of flooding in real time is crucial for flood monitoring [13]. Only rivers can be monitored effectively using permanent water level sensors since it is very expensive to instrument hydrological streams, which are hundreds of square kilometers in size [10]. It is not feasible to take optical measurements when floods are in full swing, and current synthetic aperture radars lack the vertical resolution needed to monitor water levels and flow using satellites remotely.

In the last several decades, remote sensing (RS) and GIS have allowed for generating and evaluating massive datasets from which more precise and useful flood hazard maps could be extracted [14-17]. However, Synthetic Aperture Radar (SAR) is a type of radar that can gather information from the air or space any time of day or night and even through clouds [18,19]. Furthermore, SAR is an active microwave RS instrument that can yield comprehensive images of Earth's surface at any time of day or night, regardless of the weather [20-22]. Floods are generally associated with heavy rain when it is nearly impossible for optical remote sensing devices to picture the water. However, the ability of sensors to detect water through cloud cover makes an airborne or satellite SAR system an effective tool for flood monitoring [23]. Emphasis on that, SAR systems are now commonly employed for flood mapping and have shown to be particularly effective in smaller and medium-sized drainage basins, where flooding often subsides before weather conditions improve [24,25]. Sentinel 1 SAR imagery offers great potential for detecting flooded areas and providing flood-related information, according to an assessment of the relevant literature.

In the early 1980s, the first techniques and algorithms for using SAR to detect flooding were created [26]. Flood mapping using SAR images employs a variety of methodologies, such as fully automated, semi-automated, hybrid, and manual approaches [27,28]. Several approaches have been examined to map the flash flood efficiently, including the Difference Index (DI), Normalized Change Index (NCI), Ratio Index (RI), Split window, Fuzzy logic, and thresholding algorithms [29-35]. Furthermore, SVM, Random Forest, Neuro-Fuzzy, and ANN are among the supervised machine-learning approaches examined for flash flood detection mapping [36,37]. Various automated thresholding approaches have been developed to aid in flash flood mapping, such as the techniques devised by OTSU, Tsai, Kapur, Kittler, and regression-based optimal thresholds. The primary aim of this study is to determine the magnitude of the flooded region during a specific flash flood incident by analyzing a sequence of Sentinel-1 images captured before and after the flash flood. Furthermore, two distinct approaches, NCI and RI, have been employed to detect the flash flood. The efficacy of the adopted methodology has been verified against the ground truth data from the flash flood induced by excessive rainfall in Erbil City on 17 December 2021.

2. Study area

Erbil, located in northern Iraq, is included in the scope of this research. Its coordinates are 36°11′28″N and 44°0′33″E on a map, as shown in Figure 1. Physically, the region consists of a wide plain with some hills to the east that are up to 426 meters above sea level [38] quaternary sediments deposited there by weathering and erosion of nearby highlands blanket the area. The quaternary sediments in the north and northeast of the study region cover the molasses-based Bai Hassan formation. The middle parts are mostly flat, whereas the northeast and east feature more rugged terrain [39]. However, Erbil experiences low summer and moderate winter humidity due to its semiarid environment. Temperatures exceeding 45 °C are common in the summer, while lows below 0 °C are common in the winter, and the weather is generally cool and wet. Yearly, it rains more than 400 mm on average [40]. It usually begins to rain around the middle of October and continues into May.

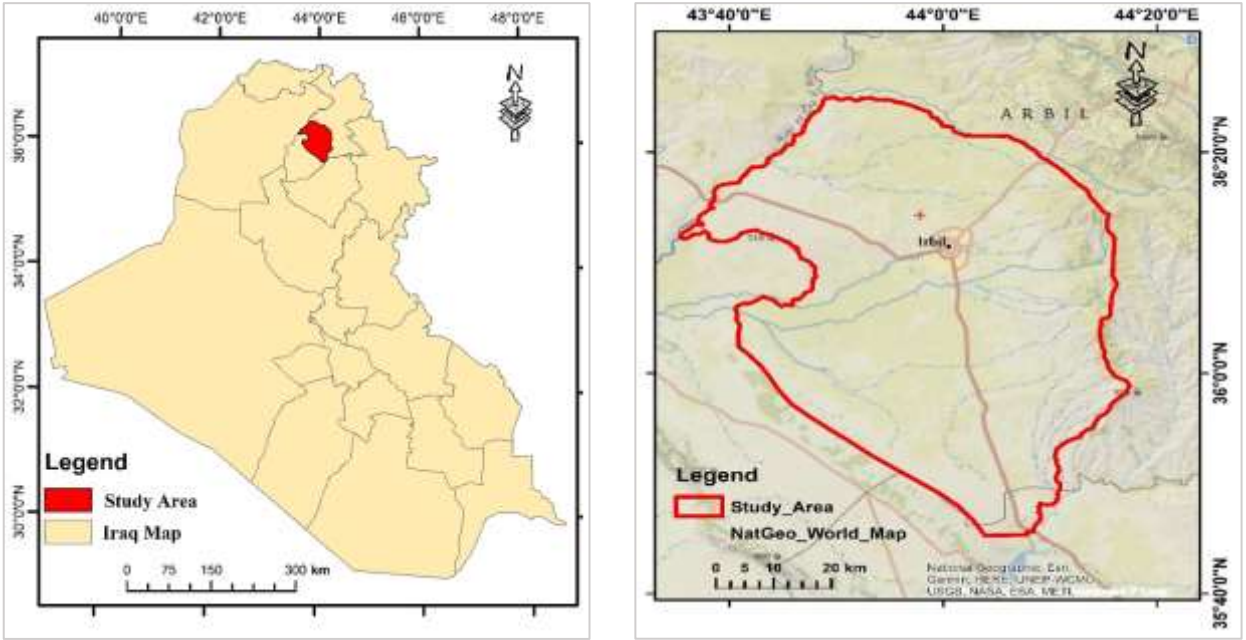

Figure 1: The study area (Erbil City)

3. Methodology

The following sections provide a detailed account of the procedures used to conduct this study. The overall flow diagram of the research approach consists of three stages: data pre-processing, change detection analysis, and accuracy assessment. Figure 2 shows the workflow for this study to detect flash floods in the study area.

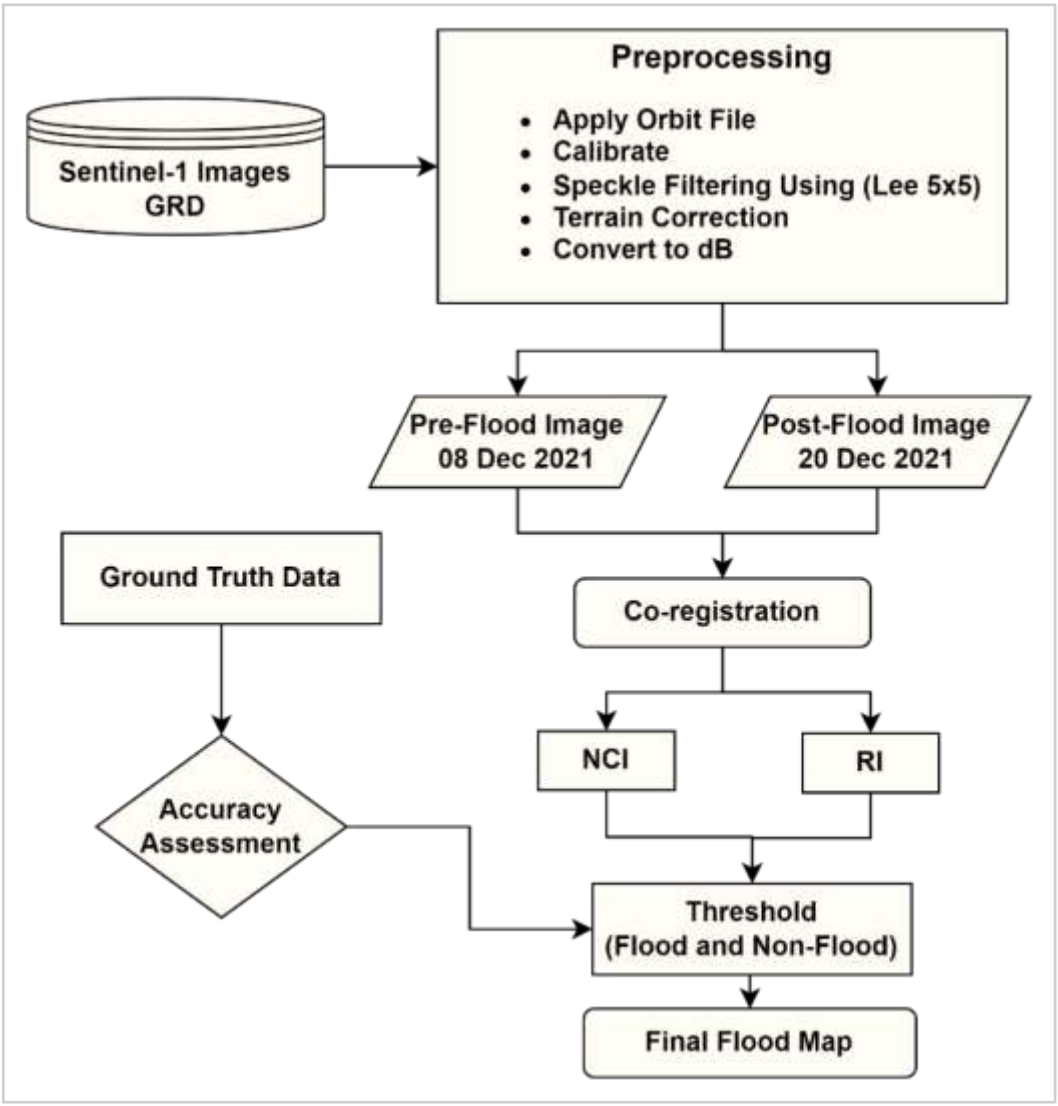

Figure 2: Workflow for the flash flood detection

3.1 Data acquisition

For both flood detection and flood mapping, it is necessary to collect two distinct sets of remotely sensed data: an image acquired prior to the flood and an image collected during the flood or after the flood. Microwaves are a type of long-wave used by SAR systems; they can travel through obstacles like clouds, vegetation, light precipitation, dense fog, and even snow. SAR is also useful for monitoring floods because of the frequent updates it provides. European Space Agency's (ESA) Sentinel-1 is a polar-orbiting imaging mission with superior spatial and temporal resolution [41]. However, the Sentinel-1A data package is a single-look, intense, Ground Range Detected (GRD) data set. The Sentinel-1A imaging radar operates in the C-band, with a frequency range of 8-4 GHz (3.75-7.5 cm wavelength) to give continuous, all-weather, day-and-night images. Table 1 details the SAR data acquisition for the study area.

Table 1: SAR data specification acquisition

Satellite	Capture date	Beam	Processing level	Resolusion class (HR/M)	Polarization	Swath Width	pixel *pixel
Sentinel-1	Pre-flood 8-12-2021	Interferometric wide swath (IW)	Level 1	HR	Single - VV	250 KM	10M * 10M
Sentinel-1	Post-flood 20-12-2021	Interferometric wide swath (IW)	Level 1	HR	Single - VV	250 KM	10M * 10M

3.2 Data pre-processing

The Sentinel's Application Platform (SNAP), a free and open-source collection of ESA Toolboxes with a common architecture, was utilized to extract EO data. Images captured by Sentinel-1 C-band SAR before and after a flood are referred to as Reference Images and Flood Images, respectively. The data was prepared for analysis in the first phase. A subset of the images was taken first to reduce and simplify the data volume. The images were calibrated by comparing values from backscatter measurements with a known standard value. Later, we applied a 5x5 pixel window Lee filter to suppress speckle noises in the images. The histogram consisted of a peak whose size varied from case to case: low values showed areas with water while high ones without water. Tow approaches were taken to identify the flooded region. A band math equation was utilized to evaluate the flood image in conjunction with a manually established threshold value of radar backscatter to determine if a specific raster pixel was inundated. The second strategy involved comparing the reference image with the flood image. A change detection methodology was utilized to differentiate between water and land.

3.3 Change detection indices

The calculation of change detection in this research involves using the normalized change index (NCI) and Ratio Index (RI). Equation 1 shows how to normalize the absolute change between pre and post-flood data to get the Normalized Change Index (NCI) [32,33].

$$NCI = \frac{\sigma^o_{vv(post-flood)} - \sigma^o_{vv(pre-flood)}}{\sigma^o_{vv(post-flood)} + \sigma^o_{vv(pre-flood)}} + 1 \quad (1)$$

where the post-flood image is represented by σ°vv(post-flood), which is the VV polarization backscatter coefficient (BSC) of the SAR image (20 December 2021). In contrast, σ°vv (pre-flood) represented the pre-flood BSC of VV polarization (8 December 2021). The NCI values range between -1 to 1, and the value is less than 0, indicating no change in both images [32]. In contrast, the positive change in the NCI values indicates the areas affected by flooding. The second approach employed in this research is RI, which stands for Ratio Index. The Ratio Index (RI) is calculated by dividing the absolute values of the flooded image by those of the pre-flood image, as given in Equation 2.

$$RI = \frac{\sigma^o_{vv(post-flood)}}{\sigma^o_{vv(pre-flood)}} \quad (2)$$

The range of RI values is from -2 to 3, with the values less than 1 indicating no change in both images. In comparison, the locations impacted by flooding are represented by positive alterations in the RI values [33].

3.4 Threshold calculation of flood and non-flood

According to Equation 1, the values of the NCI images' pixels should fall between -1 to +1. However, the NCI images barely include pixel values outside of this range. Hence, any pixel value outside this range is assigned a value of NaN. Any NCI image value below zero indicates no change, whereas any above zero indicates flood zones [33].

3.5 Validation

All the extracted flooded and non-flooded regions were checked using separate validation datasets. The validation datasets were obtained from the Ministry of Agriculture and Water Resources, General Directorate of Water Resources, and Directorate of Irrigation (Erbil) collection. The validation points had to cover the full image. As a result, obtaining the confirmation pixels from all over the area was a major challenge. Around 74 validation points were chosen using a basic random sampling technique. The next step was the construction of confusion matrices for every image. However, the confusion matrix is commonly utilized to evaluate the efficacy of multi- or binary classes. The confusion matrix was used to compute the kappa coefficient, overall accuracy, producer accuracy, and user accuracy. The overall accuracy reveals the fraction of validation pixels that were successfully categorized. The correlation between the labeled picture and the reference data is represented by the kappa coefficient. Accuracy measures for each class are producer and user accuracies. In this case, the producer's accuracy in the water class shows the percentage of final image pixels accurately classified as water. The user-defined accuracy metric for this class displays the proportion of water-covered pixels in the final result.

4. Results

The severe and dynamic flood event that occurred in northern Iraq in December 2021 was monitored in this study using multi-temporal Sentinel-1 images. Flooding was experienced in Erbil on December 17, 2021. Quick mapping is necessary to ascertain the dispersion of flood risk assessment and flooding in the study region.

To map the flood inundation event, Sentinel-1 remotely sensed data from two dates: December 8, 2021, before the flood, and December 20, 2021, after the flood. This study utilized pre- and post-flood remotely sensed data from the Sentinel-1 mission, Figure 3. The pre-flood data shows a backscattering coefficient sigma naught ranging from -22.0164 to 26.7248 dB, as illustrated in Figure 3a. Meanwhile, the post-flood data shows a backscattering coefficient ranging from -21.4878 to 25.5553 dB, as shown in Figure 3b.

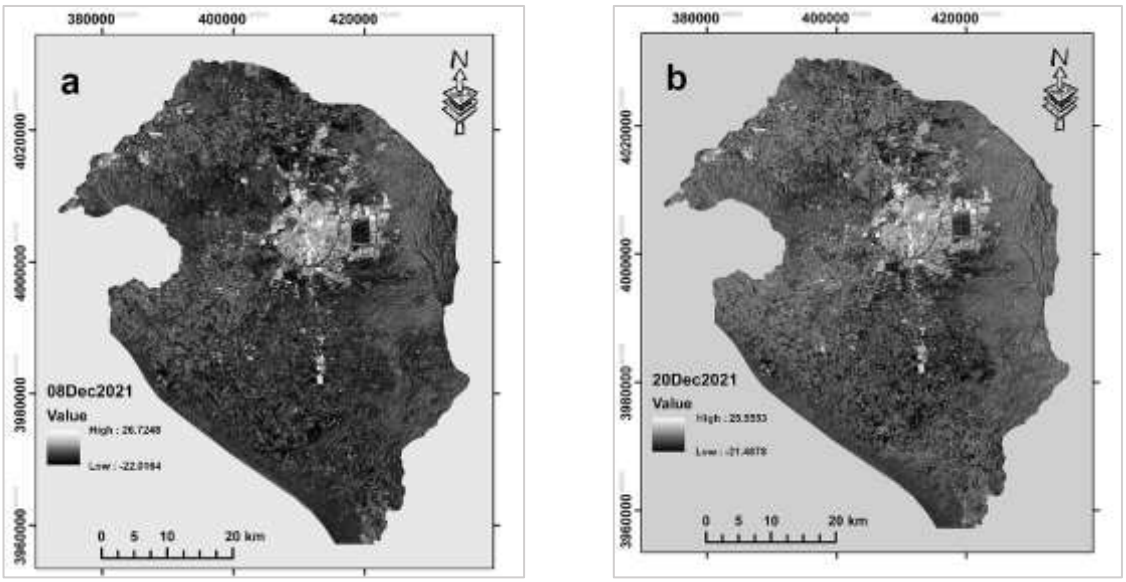

Figure 3: Temporal Sentinel-1 images (a) 08 December 2021; (b) 20 December 2021

The NCI at places is where the backscattering value changes can be quickly and accurately determined. The flash flood inundated and caused changes to the backscattering value. Figures 4 (a and b), illustrate the histogram of sigma naught of frequency and intensity by dB of both Sentinel- images before and after the flash flood.

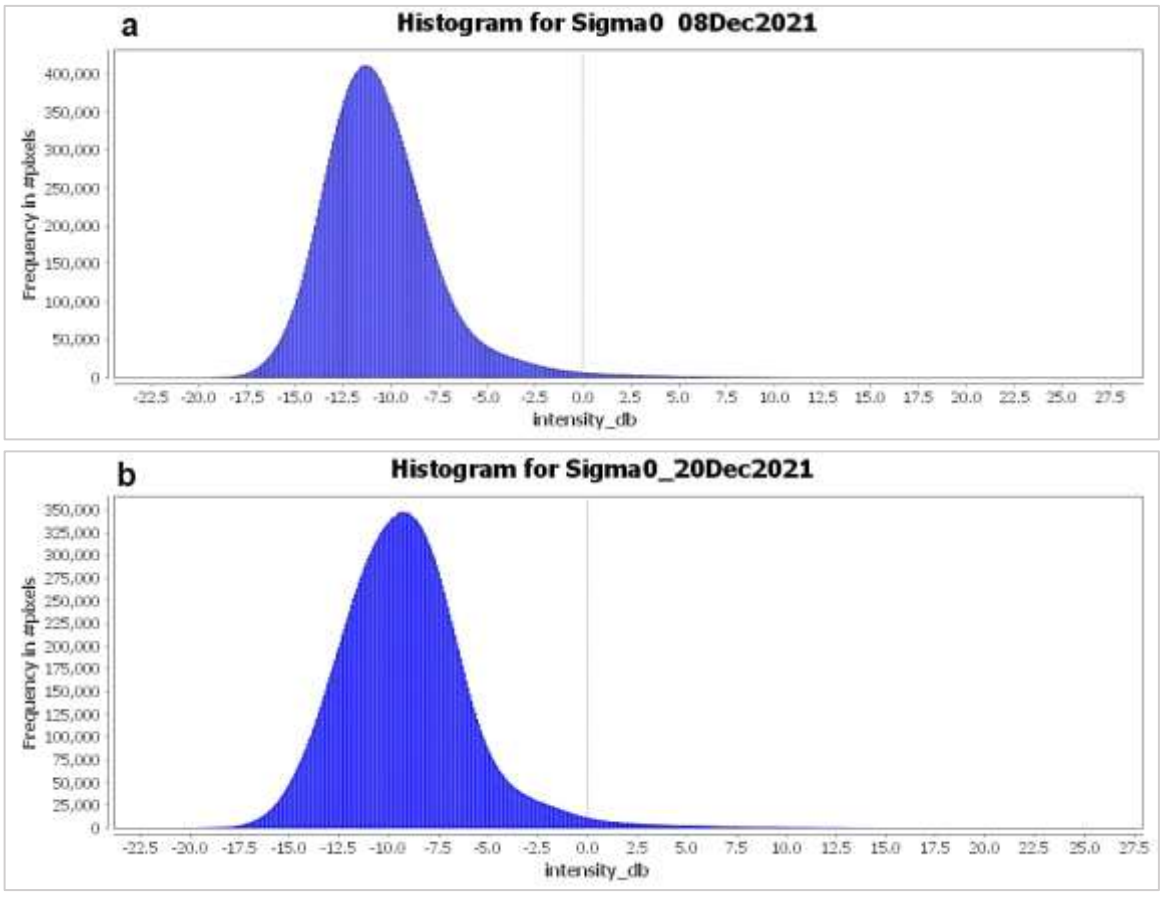

Figure 4: (a) Histogram of Sentinel-1 images (08Dec2021); (b) Histogram of Sentinel-1 images (20 Dec 2021)

The capacity of backscattering to depict changes in the position of the impacted flash flood detection allows for rather efficient and rapid NCI calculations. The range value of the change detection areas is shown to be -0.52 to 0.4 in Figure 5a, which is the outcome of the NCI. This value suggests that the likelihood of a change in surface area due to flooding increases when the NCI value decreases below 0.28 , Figure 5a.Conversely, flood damage is less likely in areas with NCI values greater than 0.28 or very vivid colors. Results of the change detection strategy utilizing the calculation of the NCI approach are shown in Figure 6a. The range of values for the change detection areas is between 0.18 and 1.95, as shown in the result of

the RI. The data indicate a higher probability of a surface area change due to flooding when the RI value falls below 1.42, Figure 5b. Simultaneously, locations with RI values greater than 1.42 or highly saturated colors are less prone to experiencing flood damage. As demonstrated in Figure 6b, the change detection strategy that utilized the RI method's calculation yielded positive results.

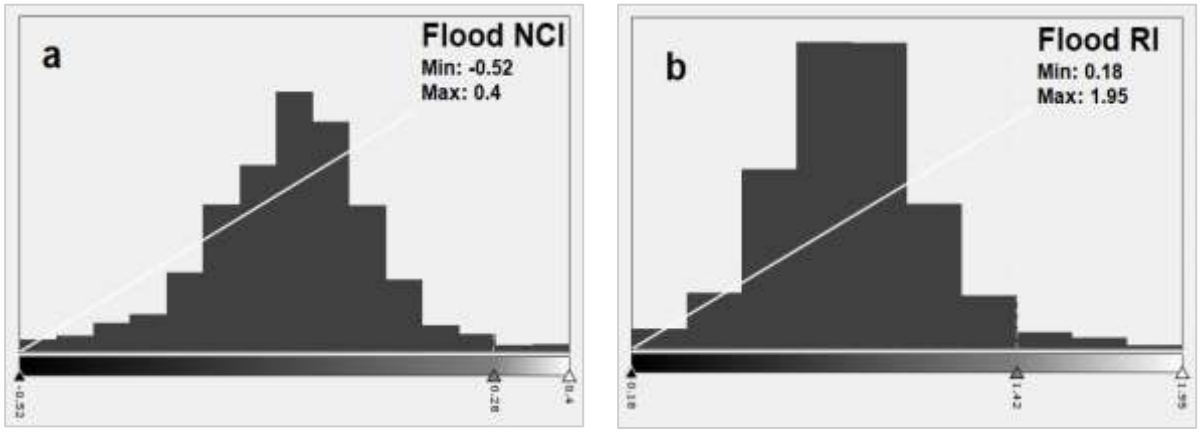

Figure 5: (a) Histogram of NCI; (b) Histogram of RI

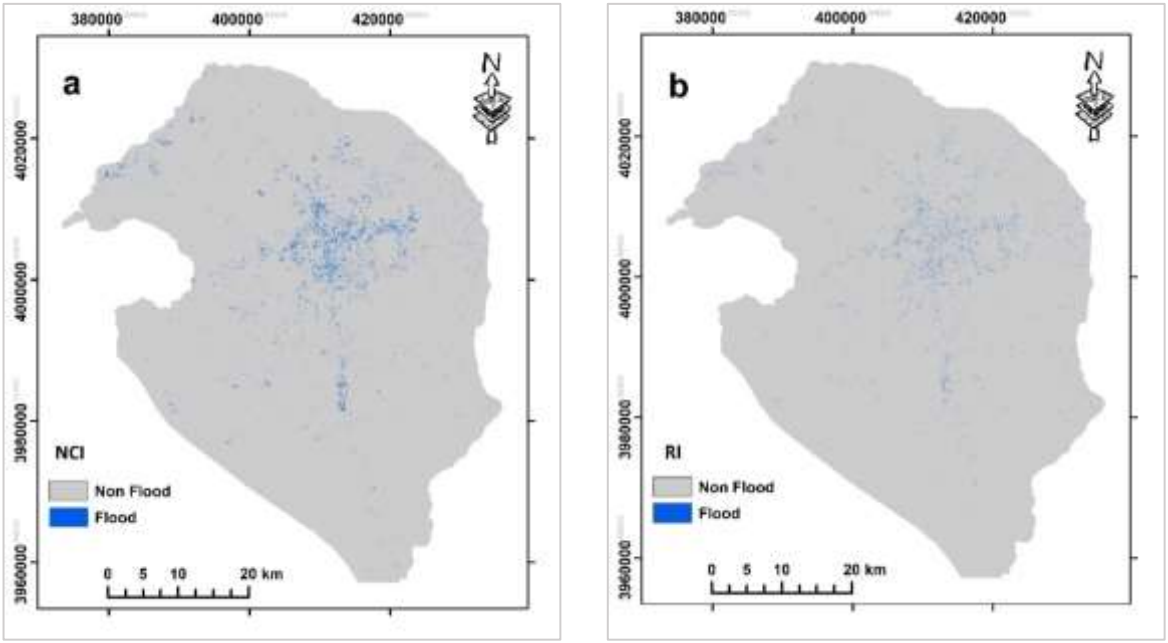

Figure 6: (a) Flood detection using normalized change index (NCI); (b) Flood detection using Ratio Index (RI)

Environmental damage caused by flood inundation events was identified using a confusion matrix and quick field observation techniques. This study needed data, images, and supplementary surveys to provide a current picture of flood-affected areas. The computation of flood hazard assessment was carried out through the overlay method embedded in a GIS environment. The images were then classified as flooded or non-flooded using the calculated threshold. Checking the accuracy of the estimated threshold in defining the flooded region was crucial. Using a basic random sampling procedure, 74 validation pixels were chosen. Comparison of binary images with independent validation datasets allowed computation of confusion matrices. The following performance measures were derived from the confusion matrices: Kappa coefficient, total accuracy, user accuracy, and producer accuracy. The computed thresholds performed admirably in terms of flooded area delineation, according to the comparative results Table 2. The NCI method yielded the best results, with a total accuracy of 90.5% and a kappa coefficient of 81.1%.

Table 2: Accuracy assessment of NCI

ClassValue	Non-Flood	Flood	Total	User Accuracy %	Kappa %
Non-Flood	37	7	44	84.1	-
Flood	0	30	30	1	-
Total	37	37	74	0	-
Producer Accuracy %	1	81.1	0	90.5	-
Kappa %	-	-	-	-	81.1

In contrast, the overall accuracy of RI was 84.3%. Therefore, NCI was shown to differentiate effectively between flooded and non-flooded regions in images taken before and after a flood. Among change detection indices, the NCI algorithm is considered one of the most efficient. Between the two indices, the NCI accurately represents the extent of the flood region. In contrast, the RI underestimates it because its calculation is based solely on the ratio of absolute values. Compared to the NCI, the flood area calculated with RI is smaller. RI may have an inflated or underinflated assessment of the flood area. Since the NCI normalizes the difference between the pre-flood and post-flood image σ° values, it also suggests that the NCI outperforms the RI in flood identification.

5. Discussion

The flood on a large scale can be monitored using Sentinel-1 imagery. The paper proposes a method based on NCI and RI that fully exploits the multi-temporal information in Sentinel-1 data for accurate detection of flash flooding. However, it is important to analyze SAR data for flash flood detection. In cases where the land surface is dark, sigma naught is small because backscattering returns a weak signal to the SAR sensor. In the interim, the high backscattering signal returned to the SAR sensor is associated with a brighter land surface condition, which accounts for the greater value of the backscattering coefficient sigma naught. The backscattering value of land use items is expected to be higher before and after floods. Figure 4, illustrates the histogram of sigma naught of frequency and intensity by dB of both Sentinel- images before and after the flash flood.

Two methodologies were examined and contrasted regarding the flood extent map they produced. Figure 6a shows the output of the first method, which employs the NCI strategy; the inundated area is white within a blue polygon, while the remaining coverage is grey. Figure 6b displays the outcome of the second approach, an image differencing method (RI), in which the flooded region is depicted in blue and is restricted with a cyan grey. The high overall accuracies demonstrate the efficiency of NCI algorithms in accurately identifying flood-affected areas from SAR images. The findings of this study indicate that SAR images are highly effective for flood inundation mapping. A quick and easy way to estimate the amount of damage caused by disasters is to utilize the results of the computations. This will enable the government to make informed decisions during times of calamity.

A quick and effective way to deal with the changing backscattering values at some places is to compute the NCI. The research region was inundated by floods, causing changes to the backscattering value. Since backscattering can depict changes in the affected flood inundation's location, NCI calculations can be employed relatively efficiently and promptly. The range value of the changed areas, as shown in Figure 5a, is the outcome of the NCI. The evaluation of the impact of flood inundation on the study location is determined appropriately. The output of the computations can be considered in future studies as a first quick step to estimating the size of disaster damage. In upcoming investigations, future ones, that is, assessment of the risk plus damage in terms of economic losses, can be calculated based on this study.

There are some limitations to this study. Data that is either real-time or almost real-time is necessary since flash floods develop rapidly. However, warnings may not be as adequate if data transmission, processing limitations, and delays occur. In this study, an image of the flash flood was obtained three days after the flash flood event, which is one of the limitations of this research. The observed flood areas are smaller than the actual flood due to the lack of an image of the exact time of the flash flood in Erbil City.

6. Conclusion

Floods are considered among the most destructive natural disasters, causing enormous economic and human suffering. Conducting ground surveys during a disaster is challenging, making RS and satellite data invaluable for hazard-related applications such as flood monitoring. Since most floods occur on cloudy days, radar systems are preferred over optical devices for data delivery and observation of floodplains. This article explores the potential of using Sentinel-1 images to track the devastating flood that struck northern Iraq in the winter of 2021. After applying the specific threshold values the NCI and RI algorithms set, the images were divided into flooded and non-flooded zones. However, the NCI was computed as a quick and effective method to address the changing backscattering values in some areas. NCI calculations were employed in a relatively efficient and timely manner. Future research on flood mapping should consider incorporating classification approaches such as machine learning and deep learning. Finally, during disaster management, this model can be used to assess the damage to vital municipal infrastructure and other regional assets.

Author contributions

Conceptualization, A. Noori and A. Ziboon; data curation, A. Noori; formal analysis, A. Noori and A. AL-Hameedawi; investigation, A. Noori; methodology, A. AL-Hameedawi; project administration, A. Ziboon, resources, A. Noori; software, A. AL-Hameedawi; supervision, A. Ziboon; validation, A. Noori and A. AL-Hameedawi.; visualization, A. AL-Hameedawi; writing—original draft preparation, A. Noori; writing—review and editing, A. Ziboon and A. AL-Hameedawi. All authors have read and agreed to the published version of the manuscript.

Funding

This research received no specific grant from any funding agency in the public, commercial, or not-for-profit sectors.

Data availability statement

The data that support the findings of this study are available on request from the corresponding author.

Conflicts of interest

The authors declare that there is no conflict of interest.

References

[1] P. M. Poortvliet, M. T. Niles, J.A. Veraart, S. E. Werners, F. C. Korporaal, B. C. Mulder, Communicating climate change risk: A content analysis of IPCC's summary for policymakers, Sustainability, 12 (2020) 4861. https://doi.org/10.3390/su12124861

[2] I. A. Alwan, N. A. Aziz, Monitoring of surface ecological change using remote sensing technique over Al-Hawizeh Marsh, Southern Iraq, Remote Sens. Appl.: Soc. Environ., 27 (2022) 100784. http://dx.doi.org/10.1016/j.rsase.2022.100784

[3] Z. K. Jabal, T .S. Khayyun, I. A. Alawn, Integrated Approach for Land Surface Temperature Assessment in Different Topography of Iraq, Eng. Technol. J., 4 (2022) 1465–1486. http://doi.org/10.30684/etj.2022.134581.1241

[4] M. M. Mansour, M. G. Ibrahim, M. Fujii, M. Naser, Sustainable development goals (SDGs) associated with flash flood hazard mapping and management measures through morphometric evaluation, Geocarto. Int., 37 (2022) 11116–11133. https://doi.org/10.1080/10106049.2022.2046868

[5] X. Tong, X. Luo, S. Liu, H. Xie,W. Chao, S. Liu, S. Liu, A. N. Makhiov, A. F. Makhiov, Y. Jiang, An approach for flood monitoring by the combined use of Landsat 8 optical imagery and COSMO-SkyMed radar imagery, ISPRS J. Photogramm Remote Sens., 136 (2018) 144–153. https://doi.org/10.1016/j.isprsjprs.2017.11.006

[6] Z. T. Abdulrazzaq, N. A. Aziz, A. A. Mohammed, Flood modelling using satellite-based precipitation estimates and digital elevation model in eastern Iraq, Int. J. Adv. Geosci., 6 (2018) 72–77. https://doi.org/10.14419/ijag.v6i1.8946

[7] H. Bourenane, Y. Bouhadad, M. Tas, Liquefaction hazard mapping in the city of Boumerdès, Northern Algeria, Bull. Eng. Geol. Environ., 77 (2018) 1473–1489. https://doi.org/10.1007/s10064-017-1137-x

[8] L. Haitham, M. Al-Mukhtar, Assessment of future climate change impacts on water resources of Khabour River catchment, north of Iraq, Eng. Technol. J., 40 (2022) 695–709. https://doi.org/10.30684/etj.v40i5.1925

[9] R. A. Atanga, The role of local community leaders in flood disaster risk management strategy making in Accra, Int. J. disaster. Risk. Reduct., 43 (2020) 101358. https://doi.org/10.1016/j.ijdrr.2019.101358

[10] H. Muhamed, M. N. Hamoodi, T. Z. Abd Alrazzak, Managing the Excess Floodwaters in the Lake Hemrin Using Remote Sensing and GIS Techniques, Eng. Technol. J., 40 (2022) 779–791. http://doi.org/10.30684/etj.2021.131195.1017

[11] V. K. Sissakian, N. Al-Ansari, N. Adamo, et al., Flood hazards in Erbil city Kurdistan region Iraq, 2021: A case study, Engineering, 14 (2022) 591–601. https://doi.org/10.4236/eng.2022.1412044

[12] S. Q. Aziz, S. M. Saleh, S. H. Muhammad, et al., Flood Disaster in Erbil City: Problems and Solutions, Environ. Prot. Res., 3 (2023) 303–318. https://doi.org/10.37256/epr.3220232993

[13] M. Mousa, X. Zhang, C. Claudel, Flash flood detection in urban cities using ultrasonic and infrared sensors, IEEE Sens. J., 16 (2016) 7204–7216. https://doi.org/10.1109/JSEN.2016.2592359

[14] D. Tien Bui, K. Khosravi, S. Li, H. Shahabi, M. Panahi, V. P. Singh, K. Chapi, A. Shirzadi, A. Shirzadi, S. Panahi, W. Chen, B. B. Ahmad, New hybrids of anfis with several optimization algorithms for flood susceptibility modeling, Water, 10 (2018) 1210. https://doi.org/10.3390/w10091210

[15] M. H. Al-Helaly, I. A. Alwan, A. N. Al-Hameedawi, Assessing land cover for Bahar Al-Najaf using maximum likelihood (ML) and artificial neural network (ANN) algorithms, J. Phys.: Conf. Ser., 2021, 12190. http://dx.doi.org/10.1088/1742-6596/1973/1/012190

[16] T. H. Shihab, A. N. Al-Hameedawi, A. M. Hamza, Random forest (RF) and artificial neural network (ANN) algorithms for LULC mapping, Eng. Technol. J., 38 (2020) 510–514. https://doi.org/10.30684/etj.v38i4A.399

[17] A. T. Ziboon, M. M. Albayati, F. T. Dalhel, Monitoring soil degradation in the Mesopotamian Plain using GIS and remote sensing techniques, Eng. Technol. J., 40 (2022) 649–660. http://dx.doi.org/10.30684/etj.v40i5.2121

[18] F. Chen, J. You, P. Tang, et al., Unique performance of spaceborne SAR remote sensing in cultural heritage applications: Overviews and perspectives, Archaeol. Prospect., 25 (2018) 71–79. https://doi.org/10.1002/arp.1591

[19] T. H. Shihab, A. N. Al-hameedawi, Desertification hazard zonation in central Iraq using multi-criteria evaluation and GIS, J. Indian Soc. Remote Sens., 48 (2020) 397–409. https://doi.org/10.1007/s12524-019-01079-2

[20] Y. Wang, L. L. Hess, S. Filoso, J. M. Melack, Understanding the radar backscattering from flooded and nonflooded Amazonian forests: Results from canopy backscatter modeling, Remote Sens. Environ., 54 (1995) 324–332. https://doi.org/10.1016/0034-4257(95)00140-9

[21] J. Sanyal and X.X. Lu, Application of remote sensing in flood management with special reference to monsoon Asia: a review, Nat Hazards, 33 (2004) 283–301. https://doi.org/10.1023/B:NHAZ.0000037035.65105.95

[22] A. N. M. Al-Hameedawi, Fuzzy Logic Approach Based on Geomatics and Remote Sensing for Siting a Petroleum Warehouse in the Metropolitan Area of Baghdad, J. Indian Soc. Remote Sens., 50 (2022) 1211–1225. https://doi.org/10.1007/s12524-022-01517-8

[23] P. A.Townsend, Relationships between forest structure and the detection of flood inundation in forested wetlands using C-band SAR, Int. J. Remote Sens., 23 (2002) 443–460. https://doi.org/10.1080/01431160010014738

[24] E. Ramsey III., A. Rangoonwala, T. Bannister, Coastal flood inundation monitoring with satellite C-band and L-band synthetic aperture radar data, J. Am. Water Resour. Assoc., 49 (2013) 1239–1260. https://doi.org/10.1111/jawr.12082

[25] G. Schumann, P. Matgen, L. Hoffmann, R. Hostache, F. Pappenberger, L. Pfister, Deriving distributed roughness values from satellite radar data for flood inundation modelling, J. Hydrol., 344 (2007) 96–111. https://doi.org/10.1016/j.jhydrol.2007.06.024

[26] R. T. Lowry, EJ L, N. A. Mudry, preliminary analysis of SAR mapping of the Manitoba flood, May 1979.

[27] L. Giustarini, R. Hostache, P. Matgen, G. J-P.Schumann, P. D. Bates, D. C. Mason, A change detection approach to flood mapping in urban areas using TerraSAR-X, IEEE Trans. Geosci. Remote Sens., 51 (2012) 2417–2430. https://doi.org/10.1109/TGRS.2012.2210901

[28] L. Giustarini, R. Hostache, D. Kavetski,M. Chini, G. Corato, S. Schlaffer, Probabilistic flood mapping using synthetic aperture radar data, IEEE Trans. Geosci. Remote Sens., 54 (2016) 6958–6969. http://dx.doi.org/10.1109/TGRS.2016.2592951

[29] J. Lim and K. Lee, Flood mapping using multi-source remotely sensed data and logistic regression in the heterogeneous mountainous regions in North Korea, Remote Sens., 10 (2018) 1036. https://doi.org/10.3390/rs10071036

[30] M. Chini, R. Hostache, L. Giustarini, P. Matgen, A hierarchical split-based approach for parametric thresholding of SAR images: Flood inundation as a test case, IEEE Trans. Geosci. Remote Sens., 55 (2017) 6975–6988. https://doi.org/10.1109/TGRS.2017.2737664

[31] V. S. K. Vanama, Y. S. Rao, Change detection based flood mapping of 2015 flood event of Chennai city using sentinel-1 SAR images, IGARSS 2019-2019 IEEE International Geoscience and Remote Sensing Symposium, IEEE, 2019, 9729–9732. http://dx.doi.org/10.1109/IGARSS.2019.8899282

[32] F. Yulianto, P. Sofan, A. Zubaidah, et al., Detecting areas affected by flood using multi-temporal ALOS PALSAR remotely sensed data in Karawang, West Java, Indonesia, Nat. Hazards, 77 (2015) 959–985. http://dx.doi.org/10.1007/s11069-015-1633-x

[33] V.S.K. Vanama, Y.S. Rao, C.M. Bhatt, Change detection based flood mapping using multi-temporal Earth Observation satellite images: 2018 flood event of Kerala, India, Eur. J. Remote Sens., 54 (2021) 42–58. https://doi.org/10.1080/22797254.2020.1867901

[34] Y. Kwak, A. Yorozuya, Y. Iwami, Disaster risk reduction using image fusion of optical and SAR data before and after tsunami, 2016 IEEE Aerospace Conference, Big Sky, MT, USA, 2016, 1–11. https://doi.org/10.1109/AERO.2016.7500520

[35] L. Pulvirenti, N. Pierdicca, M. Chini, L. Guerriero, An algorithm for operational flood mapping from Synthetic Aperture Radar (SAR) data using fuzzy logic, Nat. Hazards Earth Syst. Sci., 11 (2011) 529–540. https://doi.org/10.5194/nhess-11-529-2011

[36] X. Sun, L. Li, B. Zhang, D. Chen, L. Gao, Soft urban water cover extraction using mixed training samples and support vector machines, Int. J. Remote Sens., 36 (2015) 3331–3344. http://dx.doi.org/10.1080/01431161.2015.1042594

[37] S. A. Skakun, neural network approach to flood mapping using satellite imagery, Comput. Inform., 29 (2010) 1013–1024.

[38] M. N. M. Al- Hameedawi, Integrative GI Technology Applied to Best-Site Selection for Industrial Areas in Erbil City, Iraq, TUDpress, Verlag der Wiss, 2014.

[39] A. Ahmed, A. Al Maliki, B. Hashim, D. Alshamsi, H. Arman, A. Gad, Flood susceptibility mapping utilizing the integration of geospatial and multivariate statistical analysis, Erbil area in Northern Iraq as a case study, Sci Rep., 13 (2023) 11919. https://doi.org/10.1038/s41598-023-39290-4

[40] B. A. Ali, D. K. Mawlood, Applying the SWMM Software Model for the High Potential Flood-Risk Zone for Limited Catchments in Erbil City Governorate, Zanco J. Pure Appl. Sci., 35 (2023) 41–50. http://dx.doi.org/10.21271/ZJPAS.35.4.05

[41] M. A. Clement, C. G. Kilsby, P. Moore, Multi-temporal synthetic aperture radar flood mapping using change detection, J. Flood Risk Manag., 11 (2018) 152–168. https://doi.org/10.1111/jfr3.12303